American Mineralogist, Volume 104, pages 418–424, 2019

Sound velocities across calcite phase transitions by Brillouin scattering spectroscopy

Chao-shuai Zhao[1,2], He-ping Li[1,*], Po-fei Chen[3], and Jian-jun Jiang[1]

[1]Key Laboratory of High-Temperature and High-Pressure Study of the Earth's Interior, Institute of Geochemistry, Chinese Academy of Sciences, 550081 Guiyang, China
[2]College of Earth Sciences, University of Chinese Academy of Sciences, 100049 Beijing, China
[3]Department of Earth Sciences, National Central University, 32001 Taoyuan, Taiwan, R.O.C.

Abstract

Calcite ($CaCO_3$) is widely considered an important carbon carrier in the Earth's interior. Laboratory measurements of the velocities and elastic properties of calcite are important for understanding the deep carbon cycle. The sound velocities of calcite were determined up to 10.3 GPa at ambient temperature by Brillouin scattering spectroscopy. Dramatic decreases in the velocity of compressional wave (V_p) and shear wave (V_s) and abrupt increases in the V_p anisotropy (Ap) and maximum V_s anisotropy (As_{max}) were detected across the phase transition from $CaCO_3$-I to $CaCO_3$-II. Dramatic increases in the V_p and V_s and an abrupt decrease in Ap were observed across the phase transition from $CaCO_3$-II to $CaCO_3$-III. The phase transition from $CaCO_3$-I to $CaCO_3$-II may potentially explain the Gutenberg discontinuity at 51 km in the Izu-Bonin region. The V_p and V_s values of calcite were low. Our new results combined with literature data suggest that the low velocities of $CaCO_3$ could potentially explain the low-velocity zone occurring in northeastern (NE) Japan.

Keywords: Brillouin scattering, sound velocity, elasticity, $CaCO_3$, high pressure

Introduction

Carbonates play an important role in the transport and storage of carbon in the Earth's crust and mantle (Dasgupta and Hirschmann 2010; Sanchez-Valle et al. 2011). Calcite is widely considered one of the most important carbonates in the Earth's interior. Recent experimental and theoretical studies have shown that its high-pressure phase remains stable under lower mantle pressure and temperature conditions (Oganov et al. 2006, 2008; Ono et al. 2007; Liu et al. 2016; Dorfman et al. 2018; Li et al. 2018). The existence of calcite in the mantle is also proven by the occurrence of its inclusion in diamonds at corresponding depths (Brenker et al. 2007; Kaminsky et al. 2009; Tschauner et al. 2018). Additionally, sound velocities and elastic properties are important for understanding the structure of the Earth's interior and the causes of some abnormal behaviors (e.g., seismic wave discontinuities and low-velocity zones) (Duffy et al. 1995; Mao et al. 2010; Marcondes et al. 2016; Bayarjargal et al. 2018). Laboratory measurements of the velocities and elastic properties of calcite are thus important for determining the deep carbon cycle and identifying potential carbonate-rich regions in the Earth's interior.

Calcite crystallizes in the trigonal crystal system with space group $R\bar{3}c$ (referred to as $CaCO_3$-I) under ambient conditions. It undergoes a series of structural phase transitions into $CaCO_3$-II, $CaCO_3$-III, and $CaCO_3$-VI at ~1.5, ~2.1, and ~15.0 GPa, respectively (Catalli 2005; Merlini et al. 2012; Liu et al. 2016). There are numerous experimental and theoretical reports on the velocity and elasticity of calcite. However, these studies are mainly concentrated on low-pressure measurements with ultrasonic interferometry or high-pressure conditions modeled through theoretical calculation (Peselnick and Robie 1963; Wang 1966; Grady et al. 1978; Thanh and Lacam 1984; Zhao et al. 2009; Almqvist et al. 2010; Juneja and Endait 2017; Stekiel et al. 2017; Huang et al. 2017; Bayarjargal et al. 2018). Furthermore, some data on properties at ambient pressure and/or high-temperatures based on Brillouin scattering spectroscopy have been reported (Chen et al. 2001; Lin 2013). Therefore, we investigated the high-pressure velocities of natural calcite up to 10.3 GPa at ambient temperature by Brillouin scattering spectroscopy.

Methods

Natural single-crystal calcite (Iceland spar) samples were obtained from Guizhou, China. The composition was measured by electron microprobe analyses (JXA-8230, 15 kV and 10 nA, Northwest University, China), which indicated a homogeneous chemical composition of $CaCO_3$ with less than 0.4 mol% Mg. For simplification, we refer to it as $CaCO_3$. Single-crystal samples with optical clarity, surface smoothness, and parallelism of <30′ were chosen for Brillouin scattering measurements.

High pressures were generated by a pair of 400 μm diamond culets. The sample chamber was composed of a rhenium gasket with a pre-indented thickness of ~70 μm and a drilled hole of ~160 μm. A volume ratio of 4:1 methanol and ethanol mixture was applied as the pressure-transmitting medium for all experiments. Ruby powders and a single-crystal platelet with a thickness of ~40 μm were loaded into the sample chamber. Four independent experiments were conducted in this study. Pressures were determined by the quasi-hydrostatic ruby scale (Mao et al. 1986). The pressure uncertainties were ±0.1 GPa below 2 GPa and ±0.3 GPa between 3 and 10.3 GPa, which were estimated from the pressure measured before and after the collection of the Brillouin spectra.

Brillouin scatting spectra were collected by a Sandercock-type six-pass tandem Fabry-Perot interferometer (TFP-2, JRS Scientific Instruments) equipped with a photomultiplier detector (Count-10B, Laser Components) and a diode-pumped laser with a wavelength of 532 nm (Verdi G2, Coherent) as an excitation source. A 60° symmetric scattering geometry was adopted in all experiments. The Brillouin scattering system was calibrated before the measurements with BK7 glass and deionized water (Yoneda and Song 2005; Sanchez-Valle et al. 2013). The aggregate velocities were calculated as follows:

* E-mail: liheping@vip.gyig.ac.cn

0003-004X/19/0003–418$05.00/DOI: https://doi.org/10.2138/am-2019-6682

$$V_i = \frac{\Delta w_i \lambda}{2\sin(\theta/2)} \quad (1)$$

where V_i is the sound velocity (subscript i represents the P wave or S wave), $\Delta\omega_i$ is the measured Brillouin shift, λ represents the incident wavelength, and θ represents the angle between the incident and scattered orientations.

RESULTS AND DISCUSSION

Sound velocities and elastic properties of calcite at high pressure

The sound velocities of calcite were determined up to 10.3 GPa at ambient temperature in a 0.3–3 GPa pressure interval by Brillouin scattering spectroscopy. The 19 sets of Brillouin scattering spectra were collected in the $(10\bar{1}1)$ plane, with 10° intervals for each pressure. The intensities of the compressional wave velocity (V_p) and shear wave velocity (V_s) varied with crystallographic direction. A representative Brillouin scattering spectrum for single-crystal calcite at 1.8 GPa and 300 K is shown in Figure 1. Although calcite has the property of birefringence, given the experimental uncertainty, its effect on velocity can be neglected based on the analysis in a previous study (Chen et al. 2001).

The V_p and V_s velocities of single-crystal calcite as a function of the azimuthal angle measured from the $(10\bar{1}1)$ cleaved plane at 0.3, 1.8, and 10.3 GPa are shown in Figure 2. The V_p and V_s values varied significantly as a function of the azimuthal angle at each pressure, indicating strong elastic anisotropies of the mineral at different phases. However, the change trends of these velocities were obviously different from each other. A comparison of the velocities at 0.3 and 1.8 GPa reveals that the latter velocities were obviously less than the former velocities. The abnormal decrease in the V_p and V_s velocities at 1.8 GPa corresponded to a different structure of calcite (i.e., $CaCO_3$-II, $P2_1/c$) (Merrill and Bassett 1975). Furthermore, the change trends of the velocities at 1.8 and 10.3 GPa were obviously different, especially for V_p. At 10.3 GPa, the V_p value strictly varied as a sine or cosine trend with the azimuthal angle, which corresponded to the $CaCO_3$-III phase, and it crystallized in the triclinic space group $P\bar{1}$ (Merlini et al. 2012).

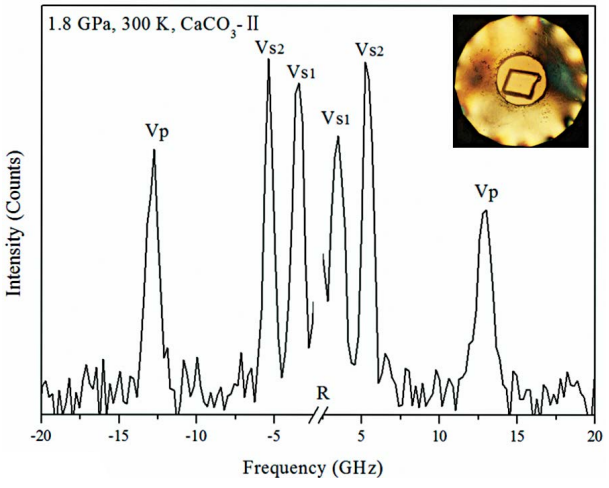

FIGURE 1. A representative Brillouin spectrum of single-crystal calcite at 1.8 GPa and 300 K. The inserted picture represents the single-crystal calcite in a diamond-anvil cell. R = Rayleigh peak. V_p and V_s stand for compressional and transverse velocities. (Color online.)

Based on the density and 19 sets of velocity data for the calcite at each pressure, the six elastic constants of calcite were calculated by a genetic algorithm using the Christoffel's equations (Chen et al. 2006; Redfern and Angel 1999). This method has been successfully used to calculate the elastic constants of magnesite, dolomite, $Zn(2\text{-methylimidazolate})_2$ (Chen et al. 2006; Tan et al. 2012), and rhodochrosite (Zhao et al. 2018). The error for each elastic constant is estimated by calculating the variations of misfit as a function of the specific C_{ij} (Chen et al. 2006).

The adiabatic bulk and shear moduli (K_s values and G), were calculated by the Voigt-Reuss-Hill averages (Meister and Peselnick 1966) using the derived elastic constants. The derived bulk and shear moduli (K_s^0 and G_0) under ambient conditions were 78.2 and 32.6 GPa, respectively, which were in agreement with previous results (see Supplemental[1] Table S1) (Chen et al. 2001; Lin 2013). Then the aggregate V_p and V_s were calculated by the following equations:

$$V_p = \sqrt{\frac{K_s + \frac{4}{3}G}{\rho}} \quad (2)$$

$$V_s = \sqrt{\frac{G}{\rho}} \quad (3)$$

The elastic constants and aggregate sound velocity properties of calcite in the form of $CaCO_3$-I at high-pressure are shown in Table 1. The monoclinic structure of $CaCO_3$-II and the triclinic structure of $CaCO_3$-III have 13 and 21 independent elastic constants, respectively, which are difficult to accurately calculate by the genetic algorithm method. This method is better used to calculate the elastic constants in orthorhombic and higher symmetry crystals.

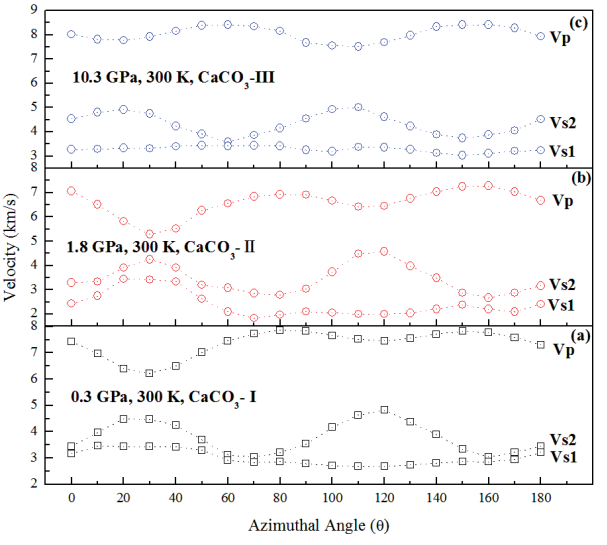

FIGURE 2. V_p and V_s are velocities of single-crystal calcite as a function of the azimuthal angle measured from a cleaved $(10\bar{1}1)$ platelet. (**a**) $CaCO_3$-I, 0.3 GPa; (**b**) $CaCO_3$-II, 1.8 GPa; (**c**) $CaCO_3$-III, 10.3 GPa. The dotted lines represent the change trends of the velocities. (Color online.)

To characterize the change trends of the velocities, as a reference, a simple average of the 19 sets of velocities at each pressure was taken as the average velocity of the calcite, as shown in Figure 3. A large discrepancy (~0.6 km/s) was apparent between the aggregate V_p and average V_p values in the $CaCO_3$-I phase, while a smaller difference was observed between the aggregate V_s and average V_s values. Dramatic decreases in V_p (–16.0%) and V_s (–18.9%) were detected across the phase transition from $CaCO_3$-I to $CaCO_3$-II, while dramatic increases in V_p (+6.6%) and V_s (+20.2%) were detected across the phase transition from $CaCO_3$-II to $CaCO_3$-III. Sharp decreases in all elastic constants and the bulk modulus of calcite were reported to occur in the phase transition from $CaCO_3$-I to $CaCO_3$-II based on ultrasonic interferometry (Thanh and Lacam 1984; Singh and Kennedy 1974). The V_p decrease (–16.0%) across the phase transition from $CaCO_3$-I to $CaCO_3$-II in this study is in good agreement with the value of –19.0% reported based on ultrasonic interferometry (Wang 1966), although there is an obvious velocity discrepancy between these two methods. The average velocities measured in this study are almost identical to the values obtained via theoretical calculation (Marcondes et al. 2016). To some extent, the change trends of the average velocities can represent the aggregate velocities. The approximate aggregate V_p and V_s values of $CaCO_3$-II were calculated based on this assumption.

The anisotropy factors for V_p and V_s are defined as follows:

$$\mathrm{Ap} = 2\times\left(V_{p,\max} - V_{p,\min}\right)/\left(V_{p,\max} + V_{p,\min}\right)\times 100\% \quad (4)$$

$$\mathrm{As} = \left(V_{s2} - V_{s1}\right)/V_s \times 100\% \quad (5)$$

where $V_{p,max}$ and $V_{p,min}$ represent the maximum and minimum V_p values of the mineral, respectively; V_{s1} and V_{s2} are two orthogonally polarized V_s values; and V_s represents the aggregate V_s value. The anisotropy factors of Ap and As_{max} of calcite are a function of pressure and are shown in Figure 4. The extrapolated Ap and As_{max} values are 24.3% and 61.4%, respectively, under ambient conditions, and these values are consistent with those in a previous study (Chen et al. 2001). The anisotropies of calcite in the different phases were considerably different, and the Ap and As_{max} of $CaCO_3$-II were much larger than those of $CaCO_3$-I and $CaCO_3$-III. Similarly, a theoretical analysis implies that there are considerable differences in the anisotropies of different phases of $CaCO_3$ (Marcondes et al. 2016; Huang et al. 2017). The Ap and As_{max} were generally stable at ~23% and ~62% in the structure of $CaCO_3$-I, respectively. Abrupt increases in Ap (+40.9%) and As_{max} (+58.4%) were detected across the phase transition from $CaCO_3$-I to $CaCO_3$-II. Within $CaCO_3$-II, the Ap ranged from 31.3% to 32.0%, and As_{max} ranged from 76.2% to 96.8%. Furthermore, across the phase transition from $CaCO_3$-II to $CaCO_3$-III, an abrupt decrease in Ap (–65.0%) was detected, and the Ap subsequently increased slowly to the maximum pressure in this study.

TABLE 1. Single-crystal elastic properties of calcite in the $CaCO_3$-I phase under high-pressure and high ambient temperature conditions

P (GPa)	0.3 ± 0.1	0.7 ± 0.1	1.0 ± 0.1	1.3 ± 0.1
C_{11} (GPa)	150.8 ± 1.5	151.8 ± 1.5	152.5 ± 1.5	153.5 ± 2.0
C_{33} (GPa)	90.2 ± 3.0	93.9 ± 3.5	93.8 ± 3.5	94.3 ± 4.0
C_{44} (GPa)	35.4 ± 0.5	39.6 ± 2.0	42.4 ± 1.5	44.9 ± 1.5
C_{12} (GPa)	63.2 ± 2.5	66.7 ± 2.5	71.2 ± 2.5	73.8 ± 3.0
C_{13} (GPa)	56.8 ± 1.5	59.2 ± 2.0	61.4 ± 2.5	63.4 ± 2.5
C_{14} (GPa)	20.0 ± 0.5	20.6 ± 0.5	21.1 ± 0.5	21.7 ± 1.0
K_s (GPa)	79.9 ± 1.7	82.5 ± 1.9	84.3 ± 2.0	85.9 ± 3.1
G (GPa)	32.8 ± 1.6	34.1 ± 2.3	34.1 ± 2.1	34.5 ± 2.5
V_P (km/s)	6.74 ± 0.11	6.84 ± 0.13	6.87 ± 0.13	6.91 ± 0.17
V_S (km/s)	3.47 ± 0.02	3.53 ± 0.03	3.52 ± 0.03	3.54 ± 0.04
Ap (%)	23.1	22.9	23.1	23.7
A_{Smax} (%)	61.5	61.6	61.7	61.2

Phase diagram of $CaCO_3$

Because the phase diagram of $CaCO_3$ is fairly complicated and phase transitions are strongly dependent on temperature, the elastic properties of calcite at ambient temperature and high-pressure are carefully applied under high-temperature and high-pressure conditions. To further discuss the geophysical implications of a suitable pressure range, we constructed a phase diagram of $CaCO_3$ with showing estimated temperature

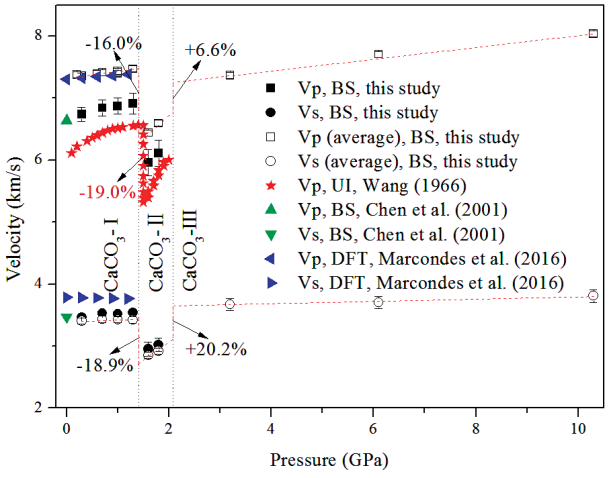

FIGURE 3. V_p and V_s are velocities of calcite as a function of pressure at ambient temperature. The dashed lines represent the tentative trend of the average sound velocities. (Color online.)

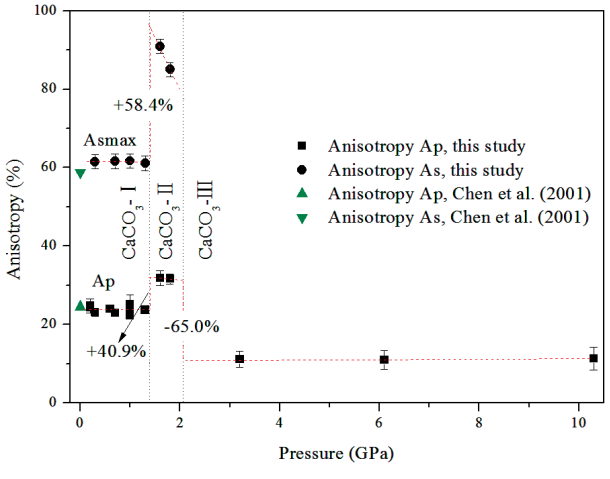

FIGURE 4. Ap and As_{max} are anisotropies of calcite as a function of pressure at ambient temperature. The dashed lines represent the tentative change trend of the anisotropies. (Color online.)

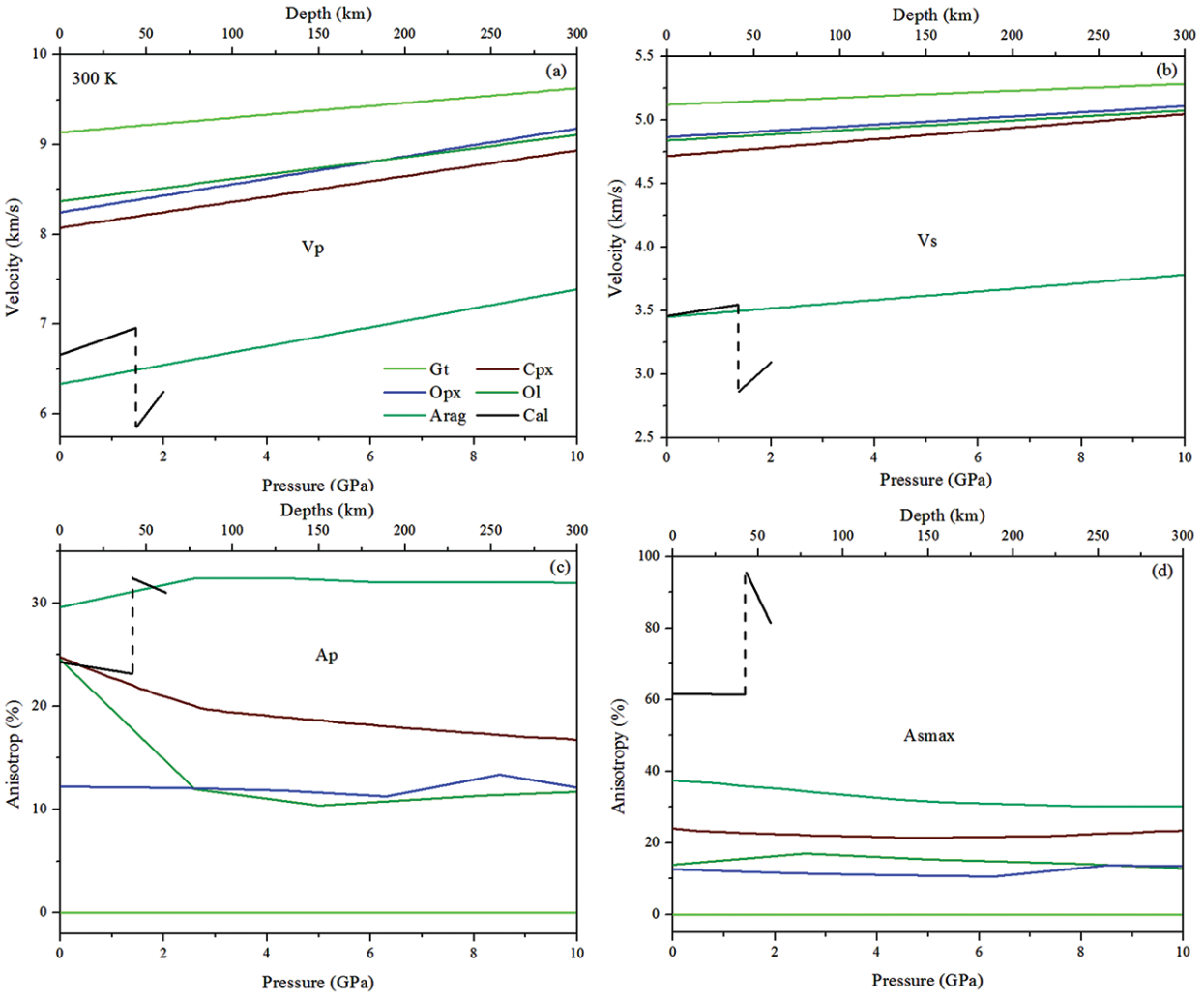

FIGURE 5. Pressure dependence of V_p (**a**) and V_s (**b**) velocities and Ap (**c**) and As_{max} (**d**) anisotropies of $CaCO_3$ and major upper mantle minerals at 300 K. Black lines = calcite (Cal) (this study; Chen et al. 2001); dark cyan lines = aragonite (Arag) (Huang et al. 2017; Liu et al. 2005; Marcondes et al. 2016); olive lines = olivine (Ol) (Mao et al. 2015; Zha et al. 1998); green lines = garnet (Gt) (Duffy and Anderson 1989; Sinogeikin and Bass 2000); wine lines = clinopyroxene (Cpx) (Duffy and Anderson 1989; Sang and Bass 2014; Collins and Brown 1998; Zou et al. 2018); blues lines = orthopyroxene (Opx) (Chai et al. 1997; Duffy and Anderson 1989). (Color online.)

and pressure conditions corresponding to relatively cold subduction zone based on the literature (Supplemental[1] Fig. S1). According to the synthesized phase diagram, calcite phases of $CaCO_3$-I, $CaCO_3$-II, and aragonite should be stable in the cold subduction zone beneath northeast (NE) Japan and Izu-Bonin (Supplemental[1] Fig. S1). Raman spectroscopy in the calcite phases showed that $CaCO_3$-II is stable between 1.4 and 2.1 GPa at ambient temperature (Supplemental[1] Fig. S2). This is consistent with the previous studies using Raman spectroscopy and X-ray diffraction measurements (Hagiya et al. 2005; Merlini et al. 2012; Liu et al. 2016; Bayarjargal et al. 2018). However, the stability field of $CaCO_3$-II should be slightly smaller at higher temperatures because of the negative Clausius-Clapeyron slopes of the phase boundary lines from $CaCO_3$-I to $CaCO_3$-II and from $CaCO_3$-II to aragonite (Liu et al. 2017; Pippinger et al. 2015). For the temperature and pressure conditions of the Izu-Bonin and NE Japan regions, $CaCO_3$-II is stable at pressures below ~1.7 GPa corresponding to 51 km depth, and then it transforms into aragonite at greater pressures. In contrast, $CaCO_3$-III may not exist under the relevant temperature and pressure conditions of the subduction zone beneath NE Japan and Izu-Bonin, since $CaCO_3$-III is stable at very low-temperature condition. Accordingly, we will focus on the velocities of $CaCO_3$-I, $CaCO_3$-II, and aragonite phases in the upcoming discussion.

Velocities and anisotropies of $CaCO_3$ and major upper mantle minerals at high pressure

The velocities and anisotropies of $CaCO_3$ and major upper mantle minerals are shown as a function of pressure in Figure 5. Comparisons are limited to room temperature and high pressure due to limited knowledge in the temperature effects on the elastic properties of $CaCO_3$. Combined with the elastic proper-

ties of aragonite reported previously (Huang et al. 2017; Liu et al. 2005; Marcondes et al. 2016), $CaCO_3$ polymorphs have the lowest V_p and V_s values and the largest Ap and As_{max} values among the major upper mantle minerals over the entire pressure range (see Fig. 5).

Velocities of the carbonated eclogite and peridotite models

To further evaluate the effect of carbonate on the velocity of the major upper mantle minerals, we calculated the velocities of eclogite and peridotite with and without 10 wt% carbonate as reported previously (Yang et al. 2014). In terms of mineral assemblage, the carbon-free eclogite model is 53.3 wt% garnet and 46.7 wt% clinopyroxene, while the carbon-free peridotite model is 59.3 wt% olivine, 12.8 wt% clinopyroxene, 11.4 wt% orthopyroxene, and 16.5 wt% garnet (Dasgupta and Hirschmann 2006; Dasgupta et al. 2004; Yang et al. 2014). Here we modeled velocities of hypothetical $CaCO_3$-rich mantle rocks, which are constructed by 90 wt% of eclogite/peridotite and 10 wt% of $CaCO_3$. Compared to the carbon-free eclogite, the V_p and V_s values decrease by 2.3% and 3.0% for $CaCO_3$-I, 3.6% and 4.4% for $CaCO_3$-II, and 2.7% and 3.0% for aragonite, respectively. Velocities significantly increase (V_p +1.3% and V_s +1.4%) during phase transition from $CaCO_3$-I to $CaCO_3$-II. Similarly, the V_p and V_s values of the carbonated peridotite decrease by about 2–4% compared to normal peridotite (see Fig. 6).

Implications

Discontinuities in seismic wave velocities are closely related to phase transitions, rapid variations in chemical composition with depth, or changes in the degree of anisotropy (Stixrude 2015). Sharp increases in V_p (+2%) and V_s (+9%) from aragonite to $CaCO_3$-VII at 25 GPa (~690 km depth) and decreases in V_p (–12%) and V_s (–3%) from $CaCO_3$-VII to post-aragonite at 40 GPa (~1010 km depth) were previously determined based on density functional theory calculations (Bayarjargal et al. 2018). According to previous study (Bayarjargal et al. 2018), seismic wave velocities increase (V_p +0.4% and V_s +0.9%) upon aragonite to $CaCO_3$-VII phase transition at 25 GPa in pyrolite with 10 mol% of $CaCO_3$, while these values largely decrease (V_p –4.7% and V_s –7.0%) during $CaCO_3$-VII to post-aragonite transition at 40 GPa. These data imply that the presence of $CaCO_3$ may contribute to the discontinuities at ~700 km and 930–1120 km (Bayarjargal et al. 2018; Yang and He 2015; Kaneshima 2013).

In this study, we measured the elastic properties of calcite at pressures up to 10.3 GPa and observed dramatic decreases in V_p (–16.0%) and V_s (–18.9%) across the phase transition from $CaCO_3$-I to $CaCO_3$-II, which occurred at ~1.4 GPa (42 km depth). If eclogite or pyrolite contain 10 wt% of $CaCO_3$, seismic wave velocities significantly decrease by V_p –1.3% and V_s –1.4% upon the phase transition at 42 km depth (Fig. 6). The sharp decreases in the V_p and V_s values of $CaCO_3$ across the phase transition may be related to the Gutenberg discontinuity at ~51(±10) km, where the V_s changes by –7.8%, as reported by seismic observations in the Izu-Bonin region (Revenaugh and Jordan 1991). On the other hand, we observed abrupt increases in Ap (+40.9%) and As_{max} (+58.4%) across the phase transition. A small amount of calcite-type carbonates can significantly modify the seismic anisotropy of rocks (Valcke et al. 2006; Lin 2013). A strong, localized anisotropy is also considered to explain the Gutenberg discontinuity (Gung et al. 2003; Stixrude 2015). If calcite exists in the Izu-Bonin region in a sufficient quantity, the phase transition from $CaCO_3$-I to $CaCO_3$-II may represent a possible explanation of the Gutenberg discontinuity at 51 km in this region.

A low-velocity layer has been observed in NE Japan, and it extends to 150 km depth beneath this region (Matsuzawa et al. 1986; Hasegawa et al. 1994; Peacock 2003). Under the relevant temperature and pressure conditions of the NE Japan region,

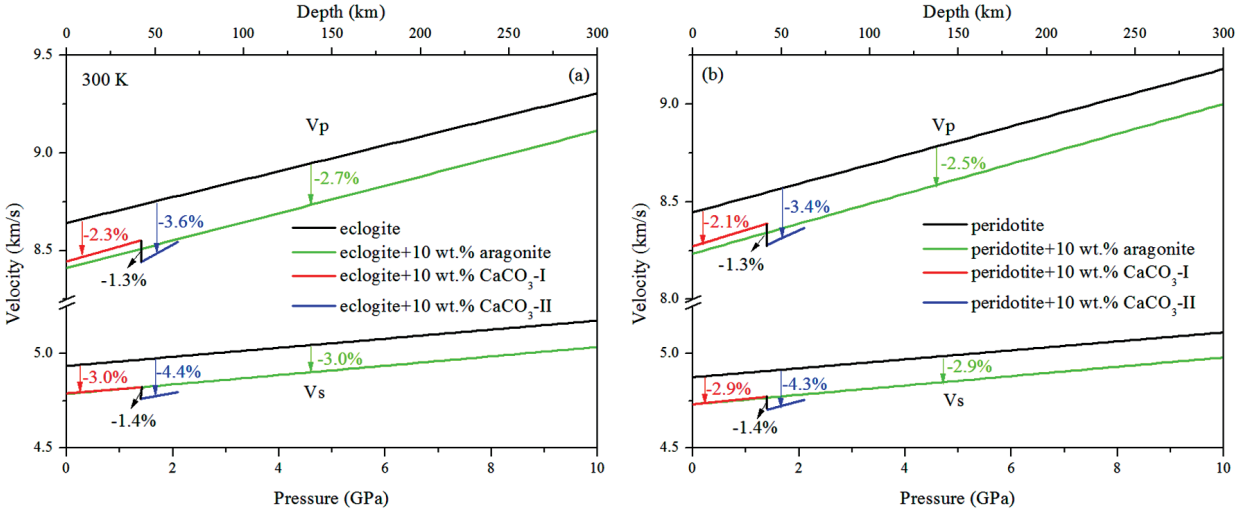

Figure 6. V_p and V_s are velocities of eclogite and peridotite models with and without $CaCO_3$ at ambient temperature: (**a**) eclogite model; (**b**) peridotite model. In terms of mineral assemblage, the carbon-free eclogite model is 53.3 wt% garnet and 46.7 wt% clinopyroxene, while the carbon-free peridotite model is 59.3 wt% olivine, 12.8 wt% clinopyroxene, 11.4 wt% orthopyroxene, and 16.5 wt% garnet (Dasgupta and Hirschmann 2006; Dasgupta et al. 2004; Yang et al. 2014). The carbonated eclogite and peridotite models include 10 wt% $CaCO_3$ ($CaCO_3$-I, $CaCO_3$-II, aragonite), respectively. (Color online.)

the velocities of $CaCO_3$, including $CaCO_3$-I, $CaCO_3$-II, and aragonite, are much slower than those of the major upper mantle minerals up to at least 10 GPa (300 km depth) (see Figs. 5a and 5b). As described above, we estimated sound wave velocities of mantle rocks (eclogite and peridotite) containing 10 wt% of $CaCO_3$ (Fig. 6). Results show that velocities significantly reduced by enrichment of $CaCO_3$ up to –4.4% compared to normal mantle. The presence of $CaCO_3$ at relevant depths in the NE Japan region may potentially explain the low-velocity zone observed in this region. In addition, a previous study suggested that the sound velocities of $CaCO_3$ in the post-aragonite phase were much lower than those of the major lower mantle constituent $MgSiO_3$, and the presence of $CaCO_3$ was considered a possible way to explain the existence of the low-velocity region in the bottom of the lower mantle (Marcondes et al. 2016). The low velocities and large anisotropies of carbonates (see Supplemental[1] Fig. S3 and reference in Marcondes et al. 2016) can be considered potentially useful features for detecting carbonate-rich regions in the Earth's crust and mantle, which further improve our knowledge of the deep carbon cycle and seismic observations in the Earth's interior.

Funding

This work was supported by the Strategic Priority Research Program (B) of the Chinese Academy of Sciences under Grant XDB18010401 and Major State Research Development Program of China under Grant 2016YFC0601101.

Acknowledgments

We very appreciated two anonymous reviewers and editors for their suggestions and comments, which greatly improved the manuscript. We acknowledged Changsheng Zha for the guidance and advice on the experiment. We also thanked Wenqiang Yang for the help of electron microprobe measurements.

References cited

Almqvist, B.S.G., Burlini, L., Mainprice, D., and Hirt, A.M. (2010) Elastic properties of anisotropic synthetic calcite-muscovite aggregates. Journal of Geophysical Research, 115, B08203.

Bayarjargal, L., Fruhner, C.-J., Schrodt, N., and Winkler, B. (2018) $CaCO_3$ phase diagram studied with Raman spectroscopy at pressures up to 50 GPa and high-temperatures and DFT modeling. Physics of the Earth and Planetary Interiors, 281, 31–45.

Brenker, F.E., Vollmer, C., Vincze, L., Vekemans, B., Szymanski, A., Janssens, K., Szaloki, I., Nasdala, L., Joswig, W., and Kaminsky, F. (2007) Carbonates from the lower part of transition zone or even the lower mantle. Earth and Planetary Science Letters, 260, 1–9.

Catalli, K. (2005) A high-pressure phase transition of calcite-III. American Mineralogist, 90, 1679–1682.

Chai, M., Brown, J.M., and Slutsky, L.J. (1997) The elastic constants of an aluminous orthopyroxene to 12.5 GPa. Journal of Geophysical Research, 102, 14,779–14,785.

Chen, C.-C., Lin, C.-C., Liu, L.-G., Sinogeikin, S.V., and Bass, J.D. (2001) Elasticity of single-crystal calcite and rhodochrosite by Brillouin spectroscopy. American Mineralogist, 86, 1525–1529.

Chen, P.-F., Chiao, L.-Y., Huang, P.-H., Yang, Y.-J., and Liu, L.-G. (2006) Elasticity of magnesite and dolomite from a genetic algorithm for inverting Brillouin spectroscopy measurements. Physics of the Earth and Planetary Interiors, 155, 73–86.

Collins, M.D., and Brown, J.M. (1998) Elasticity of an upper mantle clinopyroxene. Physics and Chemistry of Minerals, 26, 7–13.

Dasgupta, R., and Hirschmann, M.M. (2006) Melting in the Earth's deep upper mantle caused by carbon dioxide. Nature, 440(7084), 659–662.

——— (2010) The deep carbon cycle and melting in Earth's interior. Earth and Planetary Science Letters, 298, 1–13.

Dasgupta, R., Hirschmann, M.M., and Withers, A.C. (2004) Deep global cycling of carbon constrained by the solidus of anhydrous, carbonated eclogite under upper mantle conditions. Earth and Planetary Science Letters, 227(1-2), 73–85.

Dorfman, S.M., Badro, J., Nabiei, F., Prakapenka, V.B., Cantoni, M., and Gillet, P. (2018) Carbonate stability in the reduced lower mantle. Earth and Planetary Science Letters, 489, 84–91.

Duffy, T.S., and Anderson, D.L. (1989) Seismic velocities in mantle minerals and the mineralogy of the upper mantle. Journal of Geophysical Research, 94(B2), 1895–1912.

Duffy, T.S., Zha, C.-S., Downs, R.T., Mao, H.-K., and Hemley, R.J. (1995) Elasticity of forsterite to 16 GPa and the composition of the upper mantle. Nature Letters, 278, 170–173.

Grady, D.E., Hollenbach, R.E., and Schuler, K.W. (1978) Compression wave studies on calcite rock. Journal of Geophysical Research, 83, 2839–2849.

Gung, Y.C., Panning, M., and Romanowicz, B. (2003) Dissociative hydrogen adsorption on palladium requires aggregates of three or more vacancies. Nature, 422, 705–707.

Hagiya, K., Matsui, M., Kimura, Y., and Akahama, Y. (2005) The crystal data and stability of calcite III at high-pressures based on single-crystal X-ray experiments. Journal of Mineralogical and Petrological Sciences, 100, 31–36.

Hasegawa, A., Horiuchi, S., and Umino, N. (1994) Seismic structure of the northeastern Japan convergent plate margin: A synthesis. Journal of Geophysical Research, 99, 22295–22311.

Huang, D., Liu, H., Hou, M.-Q., Xie, M.-Y., Lu, Y.-F., Liu, L., Yi, L., Cui, Y.-J., Li, Y., Deng, L.-W., and Du, J.-G. (2017) Elastic properties of $CaCO_3$ high-pressure phases from first principles. Chinese Physics B, 26, 089101.

Juneja, A., and Endait, M. (2017) Laboratory measurement of elastic waves in Basalt rock. Measurement, 103, 217–226.

Kaminsky, F., Wirth, R., Matsyuk, S., Schreiber, A., and Thomas, R. (2009) Nyerereite and nahcolite inclusions in diamond: evidence for lower-mantle carbonatitic magmas. Mineralogical Magazine, 73, 797–816.

Kaneshima, S. (2013) Lower mantle seismic scatterers below the subducting Tonga slab: evidence for slab entrainment of transition zone materials. Physics of the Earth and Planetary Interiors, 222, 35–46.

Li, X.-Y., Zhang, Z.-G, Lin, J.-F., Ni, H.-W., Prakapenka, V.B., and Mao, Z. (2018) New high-pressure phase of $CaCO_3$ at the topmost lower mantle implication for the deep-mantle carbon transportation. Geophysical Research Letters, 45, 1355–1360.

Lin, C.-C. (2013) Elasticity of calcite: thermal evolution. Physics and Chemistry of Minerals, 40, 157–166.

Liu, L.-G., Chen, C.-C., Lin, C.-C., and Yang, Y.-J. (2005) Elasticity of single-crystal aragonite by Brillouin spectroscopy. Physics and Chemistry of Minerals, 32(2), 97–102.

Liu, J., Caracas, R., Fan, D.-W, Bobocioiu, E., Zhang, D., and Mao, W.L. (2016) High-pressure compressibility and vibrational properties of $(Ca,Mn)CO_3$. American Mineralogist, 101, 2723–2730.

Liu, C.-J., Zheng, H.-F., and Wang, D.-J. (2017) Raman spectroscopic study of calcite III to aragonite transformation under high-pressure and high-temperature. High Pressure Research, 37(4), 545–557.

Lu, C., Mao, Z., Lin, J.-F., Zhuravlev, K.K., Tkachev, S.N., and Prakapenka, V.B. (2013) Elasticity of single-crystal iron-bearing pyrope up to 20 GPa and 750 K. Earth and Planetary Science Letters, 361, 134–142.

Mao, H.-K., Xu, J.-A., and Bell, P.M. (1986) Calibration of the ruby pressure gauge to 800 kbar under quasi-hydrostatic conditions. Journal of Geophysical Research, 91, 4673–4676.

Mao, Z., Fan, D.-W., Lin, J.-F., Yang, J., Tkachev, S.N., Zhuravlev, K., and Prakapenka, V.B. (2015) Elasticity of single-crystal olivine at high-pressures and temperatures. Earth and Planetary Science Letters, 426, 204–215.

Mao, Z., Jacobsen, S.D., Jiang, F., Smyth, J.R., Holl, C.M., Frost, D.J., and Duffy, T.S. (2010) Velocity crossover between hydrous and anhydrous forsterite at high-pressures. Earth and Planetary Science Letters, 293, 250–258.

Marcondes, M.L., Justo, J.F., and Assali, L.V.C. (2016) Carbonates at high-pressures Possible carriers for deep carbon reservoirs in the Earth's lower mantle. Physical Review B, 94, 104112.

Matsuzawa, T., Umino, N., Hasegawa, A., and Takagi, A. (1986) Upper mantle velocity structure estimated from PS-converted wave beneath the northeastern Japan Arc. Geophysical Journal Royal Astronomical Society, 86, 767–787.

Meister, R., and Peselnick, L. (1966) Variational method of determining effective moduli of polycrystals with tetragonal symmetry. Journal of Applied Physics, 37, 4121–4125.

Merlini, M., Hanfland, M., and Crichton, W.A. (2012) $CaCO_3$-III and $CaCO_3$-VI, high-pressure polymorphs of calcite: Possible host structures for carbon in the Earth's mantle. Earth and Planetary Science Letters, 333–334, 265–271.

Merrill, B.L., and Bassett, W.A. (1975) The crystal structure of $CaCO_3$(II), a high-pressure metastable phase of calcium carbonate. Acta Crystallographica, B31, 343–349.

Oganov, A.R., Glass, C.W., and Ono, S. (2006) High-pressure phases of $CaCO_3$: Crystal structure prediction and experiment. Earth and Planetary Science Letters, 241, 95–103.

Oganov, A.R., Ono, S., Ma, Y., Glass, C.W., and Garcia, A. (2008) Novel high-pressure structures of $MgCO_3$, $CaCO_3$ and CO_2 and their role in Earth's lower mantle. Earth and Planetary Science Letters, 273, 38–47.

Ono, S., Kikegawa, T., and Ohishi, Y. (2007) High-pressure transition of $CaCO_3$. American Mineralogist, 92, 1246–1249.

Peacock, S.M. (2003) Thermal structure and metamorphic evolution of subducting slabs. In J.M. Eiler, Eds., Inside the Subduction Factory, Geophysical Monograph, 7–22. AGU Press, Washington, D.C.

Peselnick, L., and Robie, R.A. (1963) Elastic constants of calcite. Journal of Applied

Physics, 34, 2494–2495.
Pippinger, T., Miletich, R., Merlini, M., Lotti, P., Schouwink, P., Yagi, T., Crichton, W.A., and Hanfland, M. (2015) Puzzling calcite-III dimorphism: crystallography, high-pressure behavior, and pathway of single-crystal transitions. Physics and Chemistry of Minerals, 42, 29–43.
Redfern, S.A.T., and Angel, R.J. (1999) High-pressure behaviour and equation of state of calcite, $CaCO_3$. Contributions to Mineralogy and Petrology, 134, 102–106.
Revenaugh, J., and Jordan, T. (1991) Mantle layering from ScS reverberations: 3. The upper mantle. Journal of Geophysical Research, 96, 19781–19810.
Sanchez-Valle, C., Ghosh, S., and Rosa, A.D. (2011) Sound velocities of ferromagnesian carbonates and the seismic detection of carbonates in eclogites and the mantle. Geophysical Research Letters, 38, L24315.
Sanchez-Valle, C., Mantegazzi, D., Bass, J.D., and Reusser, E. (2013) Equation of state, refractive index and polarizability of compressed water to 7 GPa and 673 K. Journal of Chemical Physics, 138, 054505.
Sang, L.-Q., and Bass, J.D. (2014) Single-crystal elasticity of diopside to 14 GPa by Brillouin scattering. Physics of the Earth and Planetary Interiors, 228, 75–79.
Singh, A.K., and Kennedy, G.C. (1974) Compression of calcite to 40 kbar. Journal of Geophysical Research, 79, 2615–2622.
Sinogeikin, S.V., and Bass, J.D. (2000) Single-crystal elasticity of pyrope and MgO to 20 GPa by Brillouin scattering in the diamond cell. Physics of the Earth and Planetary Interiors, 120, 43–62.
Stekiel, M., Nguyen-Thanh, T., Chariton, S., McCammon, C., Bosak, A., Morgenroth, W., Milman, V., Refson, K., and Winkler, B. (2017) High-pressure elasticity of $FeCO_3$-$MgCO_3$ carbonates. Physics of the Earth and Planetary Interiors, 271, 57–63.
Stixrude, L. (2015) Properties of rocks and minerals–seismic properties of rocks and minerals, and structure of the Earth. In A. Dziewonski and B. Romanowicz, Eds., Treatise on Geophysics: Mineral Physics, 2 ed., p. 417–421. Elsevier.
Tan, J.-C., Civalleri, B., Lin, C.-C., Valenzano, L., Galvelis, R., Chen, P.-F., Bennett, T.D., Mellot-Draznieks, C., Zicovich-Wilson, C.M., and Cheetham, A.K. (2012) Exceptionally low shear modulus in a prototypical imidazole-based metal-organic framework. Physical Review Letters, 108, 095502.
Thanh, D.V., and Lacam, A. (1984) Experimental study of the elasticity of single crystalline calcite under high-pressure (the calcite I-calcite II transition at 14.6 kbar). Physics of the Earth and Planetary Interiors, 34, 195–203.
Tschauner, O., Huang, S., Greenberg, E., Prakapenka, V.B., Ma, C., Rossman, G.R., Shen, A.H., Zhang, D., Newville, M., Lanzirotti, A., and Tait, K. (2018) Ice-VII inclusions in diamonds Evidence for aqueous fluid in Earth's deep mantle. Science, 359, 1136–1139.
Valcke, S.L.A., Casey, M., Lloyd, G.E., Kendall, J.-M., and Fisher, Q.J. (2006) Lattice preferred orientation and seismic anisotropy in sedimentary rocks. Geophysical Journal International, 166, 652–666.
Wang, C.-Y. (1966) Velocity of compression waves in limestones, marbles, and a single-crystal of calcite to 20 Kilobars. Journal of Geophysical Research, 71, 3543–3547.
Yang, J., Mao, Z., Lin, J.-F., and Prakapenka, V.B. (2014) Single-crystal elasticity of the deep-mantle magnesite at high-pressure and temperature. Earth and Planetary Science Letters, 392, 292–299.
Yang, Z., and He, X. (2015) Oceanic crust in the mid-mantle beneath west-central Pacific subduction zones: evidence from S to P converted waveforms. Geophysical Journal International, 203, 541–547.
Yoneda, A., and Song, M. (2005) Frequency domain analysis of ultrasonic velocity: An alternative bond effect correction constraining bond properties. Journal of Applied Physics, 97, 024908.
Zha, C.-S., Duffy, T.S., and Downs, R.T. (1998) Brillouin scattering and X-ray diffraction of San Carlos olivine direct pressure determination to 32 GPa. Earth and Planetary Science Letters, 159, 25–33.
Zhao, C.-S, Li, H.-P, Chen, P.-F, Jiang, J.-J, and Liang, W. (2018) Single-crystal elasticity of the rhodochrosite at high-pressure by Brillouin scattering spectroscopy. High Pressure Research, 38, 396–405.
Zhao, J., Zhou, B., Liu, B., and Guo, W. (2009) Elasticity of single-crystal calcite by first-principles calculations. Journal of Computational and Theoretical Nanoscience, 6, 1181–1188.
Zou, F., Wu, Z.-Q., Wang, W.-Z., and Wentzcovitch, R.M. (2018) An extended semi-analytical approach for thermoelasticity of monoclinic crystals: application to diopside. Journal of Geophysical Research: Solid Earth, 123, 7629–7643.

Manuscript received June 14, 2018
Manuscript accepted November 27, 2018
Manuscript handled by Ryosuke Sinmyo

Endnote:

[1]Deposit item AM-19-36682, Supplemental Material. Deposit items are free to all readers and found on the MSA website, via the specific issue's Table of Contents (go to http://www.minsocam.org/MSA/AmMin/TOC/2019/Mar2019_data/Mar2019_data.html).